Cell Stem Cell
Article

Sustained Activation of mTOR Pathway in Embryonic Neural Stem Cells Leads to Development of Tuberous Sclerosis Complex-Associated Lesions

Laura Magri,[1,4] Marco Cambiaghi,[2,9] Manuela Cominelli,[5,9] Clara Alfaro-Cervello,[6,7] Marco Cursi,[3] Mauro Pala,[8] Alessandro Bulfone,[8] Jose Manuel Garcìa-Verdugo,[6,7] Letizia Leocani,[2] Fabio Minicucci,[3] Pietro Luigi Poliani,[5] and Rossella Galli[1,*]

[1]Neural Stem Cell Biology Unit, Division of Regenerative Medicine, Stem Cells and Gene Therapy
[2]Experimental Neurophysiology Unit, Institute of Experimental Neurology
[3]Epilepsy Center, Department of Neurology
San Raffaele Scientific Institute, Via Olgettina 58, 20132 Milan, Italy
[4]Vita-Salute San Raffaele University, Via Olgettina 58, 20132 Milan, Italy
[5]Department of Pathology, University of Brescia, Spedali Civili of Brescia, 25124 Brescia, Italy
[6]Laboratorio de Neurobiología Comparada, Instituto Cavanilles, Universidad de Valencia, 46012 Valencia, Spain
[7]Laboratorio de Morfología Celular, Centro de Investigación Príncipe Felipe, CIBERNED, Valencia, Spain
[8]BioFlag Ltd, Scientific Park of Sardinia, Pula, 09010 Cagliari, Italy
[9]These authors contributed equally to this work
*Correspondence: galli.rossella@hsr.it
DOI 10.1016/j.stem.2011.09.008

SUMMARY

Tuberous Sclerosis Complex (TSC) is a multisystem genetic disorder characterized by hamartomatous neurological lesions that exhibit abnormal cell proliferation and differentiation. Hyperactivation of mTOR pathway by mutations in either the *Tsc1* or *Tsc2* gene underlies TSC pathogenesis, but involvement of specific neural cell populations in the formation of TSC-associated neurological lesions remains unclear. We deleted *Tsc1* in *Emx1*-expressing embryonic telencephalic neural stem cells (NSCs) and found that mutant mice faithfully recapitulated TSC neuropathological lesions, such as cortical lamination defects and subependymal nodules (SENs). These alterations were caused by enhanced generation of SVZ neural progeny, followed by their premature differentiation and impaired maturation during both embryonic and postnatal development. Notably, mTORC1-dependent Akt inhibition and STAT3 activation were involved in the reduced self-renewal and earlier neuronal and astroglial differentiation of mutant NSCs. Thus, finely tuned mTOR activation in embryonic NSCs may be critical to prevent development of TSC-associated brain lesions.

INTRODUCTION

Aberrantly elevated mTOR pathway activity due to mutations in the *Tsc1* or *Tsc2* gene underlies the pathogenesis of Tuberous Sclerosis Complex (TSC), a multisystem, autosomal-dominant disorder highly prevalent in children. TSC is characterized by benign, focal malformations called hamartomas, which comprise nonmalignant cells exhibiting abnormal cell proliferation and differentiation. Notably, hamartomas are also observed in the central nervous system (CNS), where they are responsible for disabling neurological clinical features, such as epilepsy, severe mental retardation, and autism, which, together with the formation of brain tumors, account for significant morbidity and mortality (Crino et al., 2006).

The neurological and neuropsychiatric manifestations of TSC are related to specific developmental abnormalities, the cortical tubers (CTs), characterized by disorganized lamination and by the presence of aberrant cells, such as dysplastic neurons, large astrocytes, and giant cells. Tubers form during embryogenesis and serve as epileptogenic foci (Holmes and Stafstrom, 2007). Other brain malformations are the subependymal nodules (SENs), i.e., asymptomatic glio-neuronal benign lesions, located in the lateral and third ventricles (Ridler et al., 2004), which develop during fetal life and often degenerate into tumors, named subependymal giant cell astrocytomas (SEGAs).

Interestingly, dysplastic neurons and giant cells express cellular markers normally detected in the stem/progenitor cells located within the embryonic ventricular zone (VZ) and the adult subventricular zone (SVZ), suggesting that these lesions may arise pathogenically from neural stem cells (NSCs) undergoing abnormal differentiation (Ess et al., 2004; Orlova et al., 2010). According to this hypothesis, CTs might be described as "ectopic" neurogenic compartments in which the mechanisms finely tuning the acquisition of functional competence are deregulated during embryonic development. Likewise, SENs and SEGAs might originate from the uncontrolled proliferation of SVZ NSCs, which proliferate abnormally during embryogenesis and acquire malignant characteristics postnatally. To date, this hypothesis has not been formally proven. Given that hyperactivation of the mTOR pathway deregulates self-renewal and multilineage differentiation of different stem cell (SC) types, such as germinal (Hobbs et al., 2010; Sun et al., 2010), epidermal (Castilho et al., 2009), and hematopoietic SCs (Gan et al., 2008),

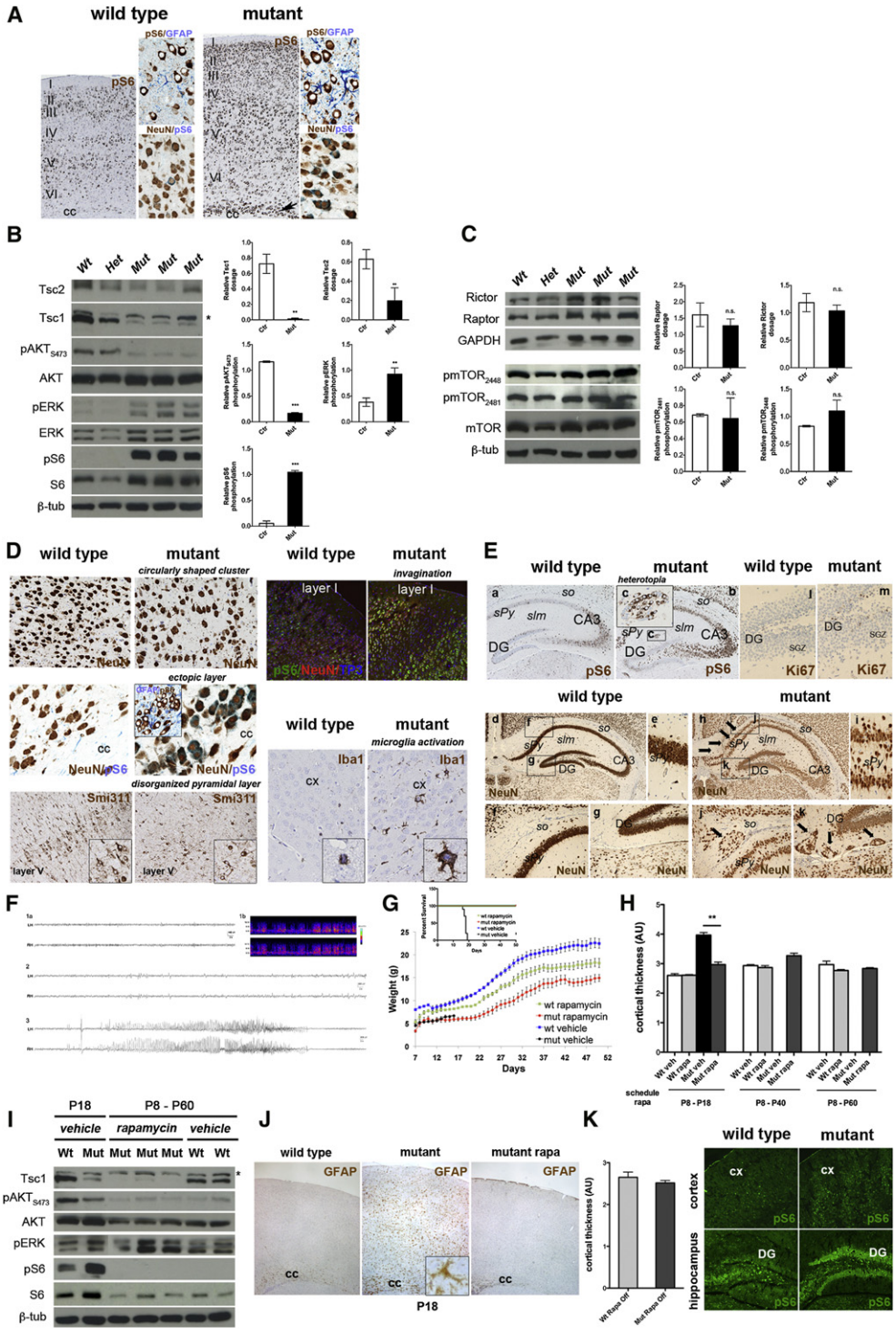

Figure 1. Targeted Inactivation of *Tsc1* in the eNSCs Results in Postnatal Megalencephaly and Cortical and Hippocampal Alterations

(A) Increased cortical thickness and pS6 staining in NeuN-immunoreactive (-IR) neuronal cells of P15 *Tsc1*$^{c/-}$*/Emx1-Cre*$^{+}$ mice. GFAP-IR cells do not express pS6. Ectopic pS6/NeuN-IR cell layer in mutant cortex is indicated by an arrow. cc, corpus callosum. Magnification 100×, insets 600×.

(B) Western blot of control and mutant cortex at P15. (*), aspecific band. Tsc1 and Tsc2 expression was normalized over β-tubulin. pAkt$_{S473}$, pERK, and pS6$_{S235/236}$ activation over the corresponding total protein (five animals per genotype) is shown.

(C) Western blot of control and mutant cortex at P15. Raptor and Rictor expression was normalized over β-tubulin, while pmTOR$_{S2481}$ and pmTOR$_{S2448}$ is shown over the corresponding total protein (five animals per genotype).

(D) IHC on P15 control and mutant cortex for pS6, NeuN, GFAP, and Smi311 (magnification 200×, inset 600×). Microglia activation in *Tsc1* mutant brains is shown by Iba-1 staining.

we set out to understand the role of mTOR in the regulation of the NSC compartment.

Recently, by targeting *Tsc1* loss in differentiating/differentiated neuronal cells (Meikle et al., 2007; Ehninger et al., 2008) and astrocytes (Uhlmann et al., 2002a), several mouse models for TSC have been generated, which, although displaying epilepsy and some cortical alterations, did not fully recapitulate the disease. Only recently, by deleting *Tsc2* in radial glial cells at E13.5, have some TSC neurological alterations been modeled (Way et al., 2009). To improve the specificity and the pathological significance of cell targeting, we generated a conditional mouse in which *Tsc1* expression was deleted at E9.5 in the *Emx1*-expressing embryonic dorsal telencephalic neuroepithelium, which gives rise to the cerebral cortex and contributes to the postnatal SVZ, i.e., the two brain regions in which CTs and SEN/SEGAs arise in patients (Gorski et al., 2002; Young et al., 2007). This conditional mouse model recapitulated several distinctive neurological features of TSC, such as alterations in cortical lamination, induction of spontaneous epileptic seizures, and development of aberrantly expanded SVZ regions, closely resembling SENs. Therefore, our mouse model might be considered a valuable preclinical model of TSC.

RESULTS

Hyperactivation of the mTOR Pathway in the Dorsal Telencephalic Neuroepithelium Interferes with Proper CNS Development

To explore the effect of *Tsc1* loss in embryonic NSCs (eNSCs), we crossed *Tsc1* floxed mice with *Emx1-Cre* mice, obtaining *Tsc1*$^{c/c}$/*Emx1-Cre*$^{+}$ and *Tsc1*$^{c/-}$/*Emx1-Cre*$^{+}$ mutant mice, which were born in Mendelian ratios and were indistinguishable from control mice until postnatal day (P)4. Starting at this time point, mutants failed to gain weight (Figures S1A–S1C, available online), and at P15 they displayed reduction in body organ size (Figure S1D) with the exception of the brain, which was enlarged and displayed reduced olfactory bulbs (OBs) and macroscopic signs of hydrocephalus (Figures S1E and S1F). By P13, mutants showed a progressive decline in activity and developed a humped posture, eventually dying with a median survival time of 18 days (Figure S1G).

A substantial conversion of the *Tsc1* conditional allele into the null allele (Figure S1H) and Cre recombination in cortical embryonic cells were demonstrated by detection of GLAST/GFP-immunoreactive (IR) cells in mutant mice carrying the Rosa-YFP allele (Figure S1I).

Targeted Inactivation of *Tsc1* in the Dorsal Telencephalic Neuroepithelium Results in Postnatal Megalencephaly, Cortical Alterations, and Epilepsy

Hyperphosphorylation of pS6$_{S235/6}$, a downstream effector of mTORC1, was observed in P15 mutant cortex in most NeuN-IR neuronal cells, whereas it was not detectable in *Cre*-recombined GFAP-IR astrocytes (Figure 1A and Figure S1). P15 mutant cortex demonstrated complete loss of Tsc1 (Figure 1B), concurrent reduction in Tsc2, and a marked increase in pS6. Of note, pAKT$_{Ser473}$ was strongly reduced in mutant cortex while pERK was increased, in agreement with ERK hyperactivation in TSC-associated lesions (Jozwiak et al., 2008). No difference in Raptor, Rictor, or pmTOR$_{Ser2448/Ser2481}$ was detected (Figure 1C). Cortex from heterozygous mice showed the same pattern of mTOR pathway activation as that of controls (Figure 1B).

As in other conditional *Tsc1*/*Tsc2* mouse models, mutant brains showed megalencephaly (Figure S1E) and increased cortical thickness (Figure 1A). In line with *Emx1*-directed Cre recombination occurring predominantly in glutamatergic neurons, pS6/NeuN-IR enlarged dysplastic neurons were identified in the Smi311-IR pyramidal cell layer and in an ectopic layer between layer VI and the corpus callosum (Figures 1A and 1D). Pyramidal neurons showed abnormal projections and disarranged neurites and axons. Abnormal invaginations of layer I and circularly shaped clusters of NeuN-IR neurons were retrieved in outermost and deep cortical layers, respectively (Figure 1D), together with enhanced activation of GFAP-positive reactive glia and microglia, and reduced myelination (Figure 1J and Figure S1N).

Both Cornu Ammonis (CA) 1 and 3 regions and the dentate gyrus (DG) of the mutant hippocampus were expanded and disorganized (Figure 1E). Neurons in the granule cell layer of the DG and in the hilus/CA1/3 regions showed weak and strong pS6 activation, respectively. Several ring heterotopias were present throughout the stratum oriens (*so*), the stratum lacunosum molecolare (*slm*), and the hippocampal fissure. A higher frequency of Ki67-IR cells was also observed in the mutant DG. Notably, hippocampal lamination was defective in mutant brains, as indicated by aberrant splitting of the stratum Pyramidale (*sPy*).

pS6-positive neurons were also detected in the arcuate (ARC) and in the ventromedial hypothalamic (VMH) nuclei of

(E) High pS6 activation was detected in the *sPy* in CA1/CA3 regions and in the hilus of DG in the mutant hippocampus. Inset (*c*) in (*b*) shows a ring heterotopia in the mutant *slm* (magnification 40×, insets 200×). Increased cell proliferation in mutant hippocampus by Ki67 is shown in (*m*). Severe lamination defects in the mutant hippocampus by NeuN are shown in (*h*), such as splitting of the *sPy* with many ectopic neurons in the *so* (arrows in *h*) and several heterotopias in *so* (arrows in *j*) and in the DG (arrows in *k*). *sPy*, stratum Pyramidale; *slm*, stratum lacunosum molecolare; *so*, stratum orens; DG, dentate gyrus; CA3, cornu ammonis 3 (magnification 40×, 100×).

(F) EEG tracing showing background activity in a representative mutant mouse (1a), density spectral array (1b), background activity with superimposed sharp waves (2), and generalized cortical seizure (3). RH and LH: right and left hemispheres.

(G) Weight gain recovery after rapamycin administration and Kaplan-Meier survival curve for vehicle- and rapamycin-treated mice (n = 11).

(H) Chronic rapamycin treatment starting at P8 reduced megalencephaly in P18, P40, and P60 mutant mice.

(I) Western blot of vehicle- and rapamycin-treated cortex at P60.

(J) Decreased expression of GFAP in P18 mutant cortex after rapamycin treatment (P8–P18). GFAP-IR cells counted in the same area field were 4.2 ± 0.8 in WT, 44.0 ± 1.9 in mutant, and 1.0 ± 0.4 in rapamycin-treated mutants ($p < 0.0001$, WT versus mutant; $p < 0.0001$, mutant versus rapamycin-treated mutants).

(K) Absence of cortical and hippocampal cytoarchitectural alterations and presence of pS6 reactivation (green) in mutant brains after rapamycin discontinuation. CX, cortex; DG, dentate gyrus.

Error bars, SEM. See also Figure S1 and Movie S1.

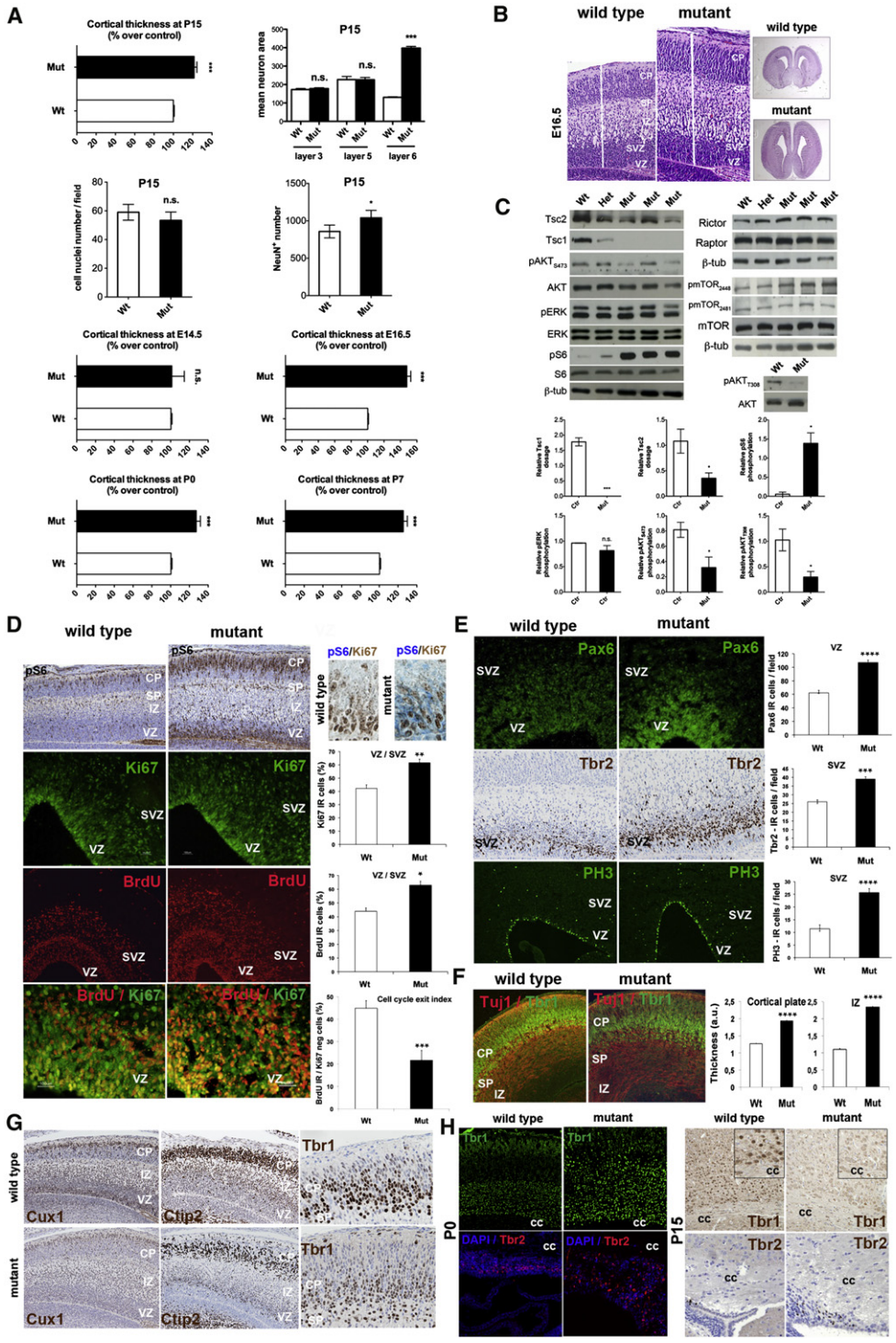

Figure 2. Deletion of *Tsc1* Deregulates Proliferation of Embryonic Cortical Progenitors and Cortical Cytoarchitecture

(A) Quantification of cortical thickness, cell size, cell density, and absolute cell number in P15 mutant and control cortex. Cell size is measured by unbiased automated cell area calculation. Cell density is measured by counting the number of nuclei in the same cortical field of controls and mutants. Absolute cell number is measured by counting NeuN-IR neurons in the same columnar fields in both control and mutant cortex. Developmental time course analyses of cortical thickness at E14.5, E16.5, P0, and P7 are shown. n.s., not significant.

(B) Megalencephaly in mutant mice at E16.5 (H&E, 200×).

(C) mTOR pathway activation in control and mutant cortex by western blot as indicated by densitometric analysis.

(D) Activation of mTORC1 (pS6) and proliferation analysis (Ki67) in VZ/SVZ progenitors. Most Ki67-IR cells are pS6-IR cells (600×). BrdU labeling experiment shows the frequency of cells exiting the cell cycle ($BrdU^+Ki67^-/BrdU^+$) (200×, 100×).

P15 mutant mice (Figure S1J), while Cre-recombined GFP-IR cells were localized in a different hypothalamic region, the anterior hypothalamic nucleus (AHP), indicating that mTORC1 activation in the ARC and VMH was non-cell-autonomous. Because mTORC1 activation in the ARC leads to decreased food intake, poor weight gain in *Tsc1*$^{c/-}$*Emx1-Cre*$^{+}$ mice could be ascribed to overactive mTORC1 signaling in the hypothalamus.

Spontaneous epileptic-like seizures were observed in 100% of our mutants at P13. Video EEG monitoring starting at P12 (n = 6; Movie S1 available online) showed that background activity in both control and mutant mice was composed of phases of 1–4 Hz or 6–9 Hz (Figures S1K and S1F). In mutants, a large spike frequently appeared just before or at the beginning of ictal activity, which was associated with generalized spike/waves, ending with a marked reduction of EEG amplitude and loss of EEG signal in case of death. Seizure length varied from 30 s to 6 min.

To assess whether mTOR pharmacological inhibition might revert the cachectic, epileptic, and megalencephalic manifestations of the mutant phenotype, we delivered rapamycin from P8 to P60. All mutant mice treated by this regimen increased in weight, stopped developing seizures, and were still alive at P60 (Figure 1G). Notably, the cortical thickness of rapamycin-treated mutant mice at P18, P40, and P60, and pS6/Akt phosphorylation at P60, were identical to that of vehicle-treated WT mice (Figures 1H and 1I). Because active cortical neurogenesis is not detected after P7, rapamycin-induced cortical thickness normalization might occur through other mechanisms, such as cortical remodeling. Indeed, rapamycin treatment from P8 to P18 induced a severe reduction in GFAP-IR reactive astrocytes (Figure 1J) and rescued the hypomyelination in mutants (Figure S1N). Within 6–10 days after rapamycin discontinuation, all mutant mice developed seizures. Although pS6 hyperactivation was still retrieved in mutants, neither did the cortical size increase back to the original mutant size, nor did the hippocampus display alterations (Figure 1K). Thus, epilepsy recurrence after rapamycin suspension might depend on perturbations of synaptic signaling in postnatal mutant neurons rather than on major cytoarchitectural abnormalities.

Deletion of *Tsc1* Deregulates Proliferation of Embryonic Cortical Progenitors and Interferes with Cortical Development

Increased cell soma size was observed only in the ectopic cell layer above the corpus callosum (layer VI) in the mutant cortex (Figure 2A), thus making it unlikely that the enlarged size of a few cells might be responsible for megalencephaly. Likewise, no difference in neuropil size and cell density could be detected. Thus, the increment in cortical thickness in mutants might be caused by excessive production of cortical cells, likely taking place during embryonic development, as shown by significantly increased NeuN-IR cells in the same columnar cortical field in mutants.

At E14.5 no differences in brain size and cortical thickness were observed, while at E16.5 both parameters were increased in mutants (n = 8, Figures 2A and 2B), which showed complete loss of Tsc1 protein, reduced level of Tsc2, increased pS6, and reduced pAkt$_{Ser473/Thr308}$ (Figure 2C). No differences were observed in ERK activation, mTOR$_{S2448/S2481}$ phosphorylation, or Rictor/Raptor expression.

In E16.5 mutant cortex, intense pS6 staining was detected (1) in the majority of progenitors located in the VZ/SVZ (Figure 2D), (2) in scattered neurons throughout the intermediate zone (IZ), (3) in the subplate (SP), (4) in cells located in the upper layers of the cortical plate (CP), and (5) in Cajal-Retzius cells in the marginal zone (MZ) (Figure S1L). A higher frequency of Ki67-IR cells was detected in VZ/SVZ, with most proliferating cells being also pS6-IR (Figure 2D). To understand whether the enhanced proliferation of mutant VZ/SVZ progenitors was associated with a decrease in the cell fraction that exited the cell cycle, we performed labeling with bromodeoxyuridine (BrdU) at E15.5 (Figure 2D). After 24 hr, the frequency of cells exiting the cell cycle (BrdU^{+} Ki67^{-}) was significantly lower in mutant VZ/SVZ than in controls, with a 20% increase in BrdU-IR cells. Interestingly, the number of Pax6-IR VZ radial glial cells (RGCs), SVZ Tbr2-IR intermediate progenitor cells (IPCs), and PH3-IR IPCs undergoing mitosis was increased in mutant cortex, suggesting that their symmetry of division was abnormal (Figure 2E). In agreement with the pS6 pattern, mutant CP and IZ were thicker (Figure 2F). Expression of Cux1, a marker of both VZ/SVZ and upper layers II–IV, was almost absent in mutant VZ/SVZ progenitors (Figure 2G). Similarly, expression of CTIP2, a marker of deep layer V, was restricted to scattered prospective mutant pyramidal neurons, suggesting premature progenitor differentiation. Tbr1-IR neurons in the SP were highly disorganized.

When the laminar structure of the cortex was analyzed perinatally, a significant expansion of Tbr1-IR neurons in layer VI was observed, suggestive of premature differentiation (Figure 2H). However, postnatally, Tbr1 expression was downregulated in aberrant layer VI cells, because these neurons might not mature properly (Figures 1A and 1C). Increased numbers of Tbr2-IR cells in the mutant dorsal SVZ were also detected at both P0 and P15.

Activation of the mTOR Pathway in eNSCs Finely Regulates Their Self-Renewal Ability

To assess the role of mTOR in NSCs ex vivo, we isolated naive cortical eNSCs by NeuroSphere Assay (NSA) at E16.5, i.e., when cortical thickness in mutants started to be significantly higher. Inhibition of mTOR by chronic rapamycin administration resulted in a remarkable reduction in NSC long-term self-renewal (Figure 3A), as mTOR inhibition interfered with growth-factor-mediated proliferative stimuli.

(E) Pax6-IR RGCs and Tbr2-IR IPCs in mutant VZ and SVZ. Quantification of the number of basal IPCs undergoing mitosis (PH3 staining) is shown (200×, 100×).
(F) IZ and CP thickness is higher in mutant cortex as shown by Tuj1 and Tbr1 staining, respectively (100×).
(G) Reduced expression of Cux1 and Ctip2 in mutant cortex. Tbr1-IR layer disorganization in mutants is evident (200×, 600×).
(H) Tbr1-IR postmitotic neurons in layer VI at P0 and P15. Tbr2-IR cells in dorsal SVZ at P0 and P15 (200×) are shown.
Error bars, SEM.

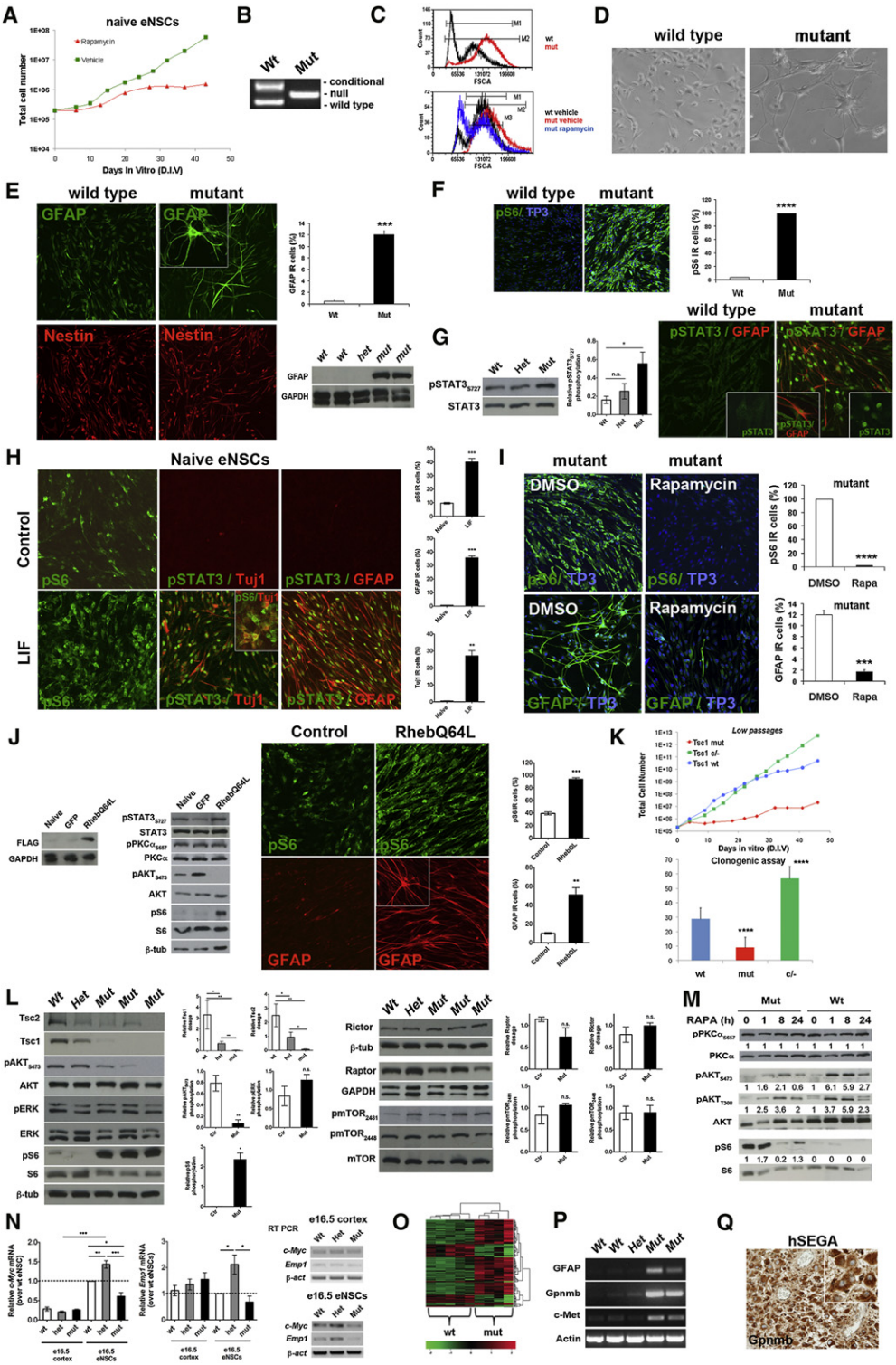

Figure 3. Activation of the mTOR Pathway in eNSCs Finely Regulates Their Self-Renewal Ability

(A) Long-term growth curve of E16.5 normal eNSCs chronically treated with vehicle (DMSO) or rapamycin (100 nM).

(B) PCR analysis of gDNA from single-embryo-derived control and mutant eNSCs, showing full recombination of the floxable allele.

(C) FACS analysis of control and mutant eNSCs, before and after 48 hr of rapamycin exposure. FSC, forward scatter.

(D) Phase contrast microphotographs of control and mutant eNSCs (400×).

(E) GFAP-IR and nestin-IR cells in undifferentiated mutant eNSCs (300×, inset 500×). Western blot for GFAP in control and mutant lines is shown.

(F) Higher pS6 phosphorylation in mutant eNSCs (300×).

Next, we established fully recombined E16.5 eNSC lines from single-embryo-derived mutant cortex (eight NSC lines per genotype) (Figure 3B). Mutant eNSCs showed increased cell size, which was reverted by rapamycin ($p < 0.005$, $n = 3$) (Figure 3C). Enlarged cell size was not detected in freshly isolated mutant E16.5 cortical cells, likely due to the very low frequency of NSCs in the E16.5 cortex in vivo (not shown). Even in the presence of EGF and FGF2, mutant eNSC cultures appeared differentiated and, in fact, comprised many abnormally enlarged GFAP-IR astrocyte-like cells (Figures 3D and 3E). Tuj1-IR neuronal cells were never retrieved in either control or mutant eNSCs. All mutant eNSCs were pS6-IR (Figure 3F).

Interestingly, strong activation of the proglial Signal Transducer and Activator of Transcription 3 (STAT3) pathway was observed upon mTOR hyperactivation, as shown by higher $pSTAT3_{Ser727}$ in mutant than in WT or heterozygous eNSCs (Figure 3G). Accordingly, nuclear translocation of mTOR-dependent $pSTAT3_{Ser727}$ and mTOR-independent $pSTAT3_{Tyr705}$ was detected only in mutant eNSCs (46.1% ± 2.5% $pSTAT3_{Ser705}$ and 47.4% ± 4.9% $pSTAT3_{Tyr705}$ -IR cells). In line with the role of STAT3 signaling in promoting GFAP expression by binding to its promoter, GFAP-IR cells in undifferentiated mutant cultures were also $pSTAT3_{Ser727/Tyr705}$ IR. To mimic the precocious differentiation of mutant eNSCs by ligand-mediated STAT3 activation, we exposed naive eNSCs to leukemia inhibitory factor (LIF) (Figure 3H). LIF addition promoted $pSTAT3_{Ser727/Tyr705}$ nuclear translocation and highly increased the fraction of pS6-IR eNSCs, indicating that STAT3 activation was mediated by enhanced mTOR activity. Most significantly, LIF-induced STAT3 activation resulted in the premature differentiation of eNSCs into neuronal and astroglial cells, which were pSTAT3 IR. Interestingly, 48 hr exposure of mutant eNSCs to rapamycin was sufficient to revert the activation of mTORC1 (Figure 3I), $pSTAT3_{Ser727}$ (not shown), and the number of GFAP-IR cells to WT levels (Figure S3).

To test whether abnormal eNSC differentiation could also be retrieved upon mTORC1 hyperactivation induced through other mechanisms, we transduced E16.5 naive eNSCs with lentiviral vectors coding for GFP (mock) or the gain-of-function mutant form of Rheb (RhebQ64L), which constitutively activates mTORC1 in a GTP-dependent manner, with no involvement of mTORC2. RhebQ64L eNSCs showed high pS6 and low $pAkt_{S473}$ (Figure 3J) and $pAkt_{T308}$ (not shown), likely through the activation of an mTORC1-dependent negative feedback loop, rather than by loss of mTORC2 activity, because phosphorylation status of the mTORC2 downstream target PKCα did not change (Figure 3J). Most RhebQ64L eNSCs were pS6 IR, did comprise a high frequency of GFAP-IR cells, and, accordingly, hyperphosphorylated $pSTAT3_{S727}$, all features that were restored to control levels by rapamycin (not shown).

Long-term self-renewal and clonal efficiency were decreased in mutant eNSCs at early passages (P2–P25), resulting in the extinction of most mutant eNSC lines (Figure 3K). However, three out of eight mutant NSC lines self-renewed efficiently for more than 25 subculturing passages, suggesting the selection of cells escaping mTOR dependence for growth, because no changes in mTOR activation were detected in low- and high-passage mutant eNSCs (Figure S2). Interestingly, inhibition of mTOR activity by chronic rapamycin in mutant eNSCs under proliferative conditions was ineffective in rescuing their reduced long-term self-renewing ability. Remarkably, although heterozygous mice did not manifest any phenotype in vivo, heterozygous eNSC lines were endowed with higher self-renewal than WT and mutant eNSCs (Figure 3K).

Each eNSC line was different in terms of mTOR activation (western blot, Table S1). Tsc1 and Tsc2 were strongly reduced, and pS6 was highly increased in all mutant cultures, with pAkt decreased in most mutant lines. pERK, mTOR, $pmTOR_{S2481/2448}$, Raptor, Rictor (Figure 3L), and $pPKC\alpha_{Ser657}$ (expression at time zero, Figure 3M) did not change. To discriminate the relative contribution of mTORC1 and mTORC2 in Akt signaling, we took advantage of both short and long treatments with rapamycin, which inhibit mTORC1 and mTORC2, respectively. One-hour and eight-hour exposures of mutant eNSCs to rapamycin strongly enhanced Akt phosphorylation on both T308 and S473, indicating the release of the mTORC1-dependent feedback (Figure 3M). Because $pPKC\alpha_{Ser657}$ did not change upon prolonged rapamycin exposure, mTORC2 was unlikely to be involved in decreased Akt_{S473} phosphorylation (Figure 3M).

Given that heterozygous eNSCs did not activate the mTOR pathway in vitro (Figure 3L), their enhanced self-renewal might relate to mTOR-independent, Tsc1/Tsc2-dependent pathways,

(G) STAT3 signaling activation upon mTOR hyperactivation, as shown by higher $pSTAT3_{S727}$ level in mutant than in WT and heterozygous eNSCs. Densitometric analysis of $pSTAT3_{Ser727}$ normalized over the relative total STAT3 protein expression (four eNSC lines per group) is shown. Immunofluorescence showing nuclear localization of $pSTAT3_{Ser727}$ in GFAP-IR cells in undifferentiated mutant eNSCs is also shown.
(H) Activation of STAT3-dependent signaling by LIF treatment results in the premature generation of Tuj1-IR and GFAP-IR cells and in mTORC1 activation (inset, Tuj1-IR cell hyperphosphorylating pS6).
(I) Exposure to rapamycin reduces the frequency of pS6-IR and GFAP-IR cells in mutant cultures.
(J) Validation of RhebQ64L transduction in eNSCs by western blot for FLAG in untransduced (naive), mock-transduced (GFP), and RhebQ64L-transduced eNSCs. mTORC1 pathway activation in RhebQ64L-transduced eNSCs, as shown by reduced $pAkt_{S473}$, and increased $pS6_{S235/6}$ and $pSTAT3_{S727}$, is demonstrated. No difference in the activation of mTORC2 was observed, as indicated by unchanged phosphorylation in $pPKC\alpha_{S657}$. Immunocytochemistry for $pS6_{S235/6}$ on control and RhebQ64L-transduced eNSC lines, the latter comprising many aberrant GFAP-IR cells, is also shown.
(K) Long-term growth curve (P5–P15) and clonal efficiency of control and *Tsc1* mutant eNSCs.
(L) mTOR pathway activation in control and *Tsc1* mutant eNSCs as indicated by densitometric analysis.
(M) Mutant and control eNSCs were treated with 100 nM rapamycin for the indicated time and analyzed by western blot for $pPKC\alpha_{S657}$, $pAKT_{S473/T308}$, and $pS6_{S235/6}$. Changes in PKCα, Akt, and pS6 phosphorylation were expressed as relative levels over untreated cells at time point 0.
(N) Quantitative and semiquantitative RT-PCR indicating increased expression of *c-myc* and its transcriptional target *Emp1* in heterozygous eNSCs.
(O) Heatmap showing the 140 differentially expressed genes (DEGs) identified by global gene expression profiling of control and mutant eNSCs.
(P) Semiquantitative RT-PCR validation of some DEGs.
(Q) GPNMB expression in human SEGA.
Error bars, SEM. See also Figure S2, Table S1, Supplemental Lists 1A and 1B, Table S2, and Figure S3.

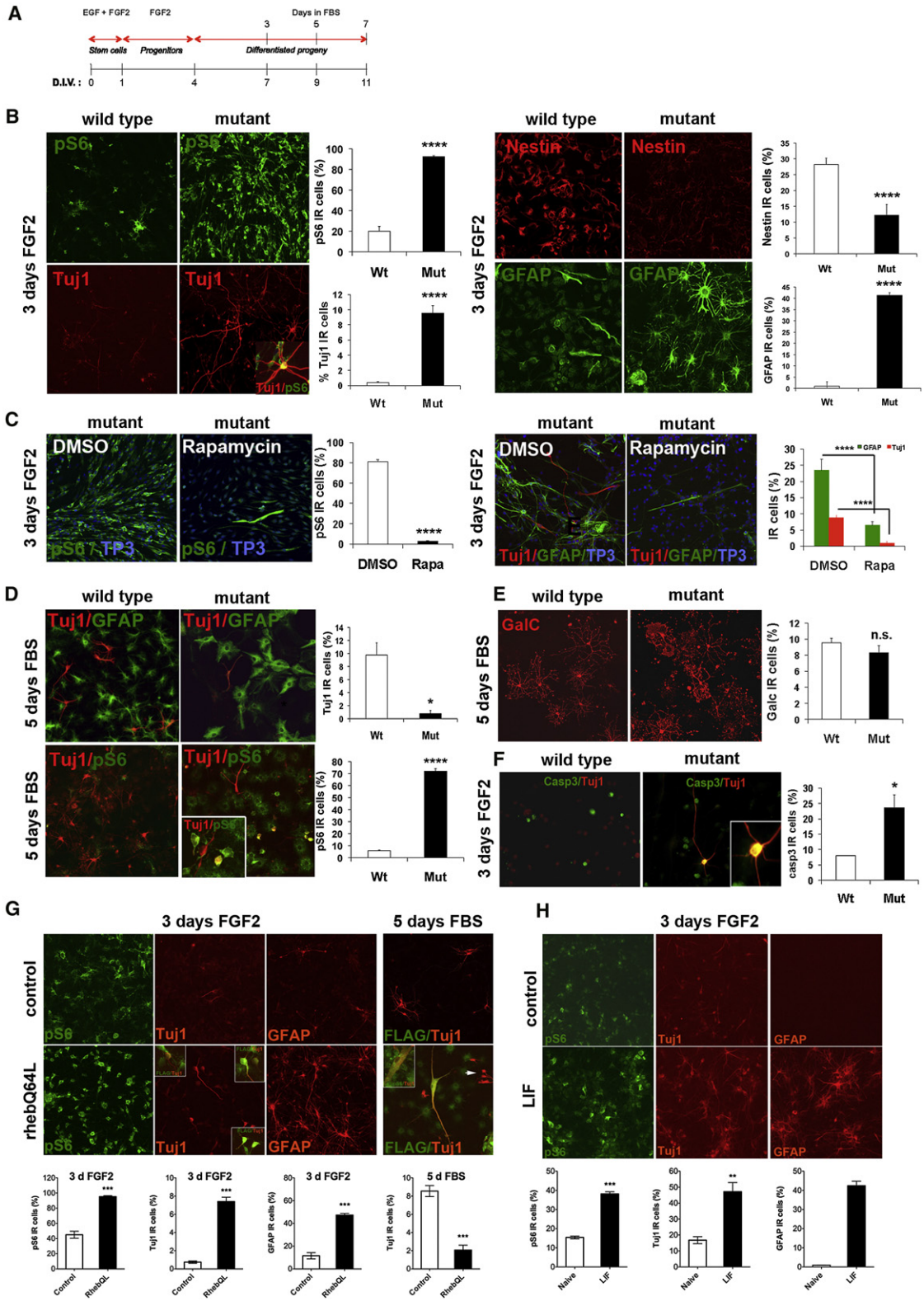

Figure 4. Activation of the mTOR Pathway in eNSCs Ex Vivo Controls their Neuronal Differentiation and Maturation

(A) Experimental paradigm for multilineage differentiation of NSCs.

(B) Tuj1-, nestin-, and GFAP-IR cells in FGF2-stimulated progenitor cultures. The majority of mutant cells were pS6 positive (300×). Inset: mutant cell coexpressing Tuj1 and pS6.

activated by mitogens. Because Tsc2 represses the cell cycle regulator *c-myc* (Schmidt et al., 2009), reduction in Tsc2 by *Tsc1* haploinsufficiency (Figure 3L and Table S1) resulted in *c-myc* overexpression (Figure 3N). Remarkably, expression of *Emp1/Tmp1*, a direct transcriptional target of c-myc and a positive regulator of cell proliferation, was also strikingly enhanced in heterozygous eNSCs (Figure 3N), suggesting that c-myc protein was functionally active. In agreement with the lack of phenotype in heterozygous mice in vivo, *c-myc* expression was similar in E16.5 WT, heterozygous, and mutant cortex, from which eNSC lines were originally established, and, overall, significantly lower than in eNSCs (Figure 3N). Because c-myc is also directly regulated by Akt, reduced pAkt in mutant eNSCs might lead to a significant decrease in *c-myc* expression in mutant eNSCs (Figure 3N) and to reduced growth in vitro. Thus, mTOR-independent and mTOR-dependent regulation of *c-myc* expression may account for the differences in self-renewal detected in heterozygous and mutant eNSCs in vitro, respectively.

WT and mutant eNSCs were also subjected to transcriptome-wide gene expression profiling, with more than 140 differentially expressed genes found (Figure 3O and List S1), some of which were also validated by RT-PCR (Figure 3P). Some top-ranking genes upregulated in mutant eNSCs (i.e., *Gpnmb*, *SerpinA3*, *S100*, *GFAP*, and *c-met*) were also highly expressed in TSC patient lesions, such as Gpnmb in SEGAs (Figure 3Q). Thus, ex vivo expanded mutant eNSCs faithfully reproduce molecular traits typical of TSC neurological lesions.

Activation of the mTOR Pathway in eNSCs Controls their Neuronal Differentiation and Maturation

WT and mutant eNSCs were induced to differentiate by withdrawal of growth factors, and to mature by the addition of fetal bovine serum (FBS), for up to a total 10 days in vitro (DIV) (Figure 4A). After culturing for 3 DIV in the presence of the sole FGF2 (a condition that drives the commitment of eNSCs into bipotent/unipotent progenitors), control eNSCs differentiated into nestin-IR progenitors, showing negligible expression of lineage-specific markers, while mutant eNSCs gave rise to a high frequency of pS6/Tuj1- and pS6/GFAP-IR cells, with remarkable decrease in nestin expression (Figure 4B and Table S2). Exposure of mutant progenitors to rapamycin greatly reduced the number of Tuj1-IR, partially that of GFAP-IR cells, and inhibited mTORC1 activation (Figure 4C).

Under maturation-promoting culture conditions, although exhibiting a normal frequency of astrocytes and oligodendrocytes (Figures 4D and 4E and Table S2), mutant cultures were almost completely devoid of neurons, as assessed by both early (Tuj1, Figure 4D) and late (MAP2, not shown) neuronal markers. Thus, continuous mTOR activation in mutant FGF2-stimulated neuroblasts in culture and lack of proper non-cell-autonomous proneuronal survival signals in the in vitro milieu inhibited their terminal maturation, leading to their apoptotic death (Figure 4F). Of note, mTOR hyperactivation in astroglial cells was not detrimental to their maturation and survival (Figure 4D and Table S2). Premature eNSC differentiation and consequent neuronal loss upon maturation were detected also in RhebQ64L eNSCs (Figure 4G). Again, LIF-mediated, mTOR-dependent STAT3 activation in FGF2-stimulated naive cultures resulted in early neuronal and astroglial differentiation (Figure 4H). To be noted, when added to maturing cells, rapamycin was ineffective in rescuing neuronal loss, suggesting the involvement of Tsc1/Tsc2-dependent, mTORC1-independent functions or rapamycin-insensitive mTORC1-dependent mechanisms in the control of late neuronal differentiation processes.

Remarkably, mTOR inhibition by chronic exposure of naive eNSC to rapamycin during differentiation resulted in the complete abrogation of neuronal production (Figure S3).

Loss of *Tsc1* Expression during Embryonic Development Severely Impairs the Organization of the Postnatal SVZ Niche

Postnatal hydrocephalus was likely caused by ependyma defects (Figure 5A). In Rosa-YFP mutant mice, putative radial glia and S100β-IR ependymal cells, at E16.5 and P15, respectively, were both GFP and pS6 IR and localized in the dorsal/medial walls of the ventricles, being absent from the lateral wall (Figure S1M and Figure 5A). As detected by electron microscopy (EM), mutant ependymal cells of the dorsal wall were larger in size and highly undifferentiated, containing large nuclei with lax chromatin, no mature nucleoli, many smooth ER cisterns, and few mitochondria. Although showing deuterosomes and basal bodies, they harbored immature and disorganized cilia. Thus, dorsally located mutant ependymal cells displayed typical features of pre-ependymal cells, suggesting that their untimely differentiation led to hydrocephalus.

Most interestingly, an aberrantly expanded SVZ region was detected in P15 mutant brains, which was reminiscent of TSC SENs, which are static, benign lesions characterized by low proliferation, scant pS6 activation, and a mixed glio-neuronal phenotype (Figures 5A and 5B). Accordingly, there were less Ki67-IR cells in the putative SEN-like region than were in controls, with no difference in the frequency of apoptotic cells (not shown). Mutant dorsal SVZ expansion contained some pS6-IR cells (Figure 5B and Table S3); many cells expressing doublecortin (DCX), Tuj1, and PSA-NCAM (Figure 5B and not shown), also organized as small heterotopic clusters; and

(C) pS6, Tuj1, and GFAP expression in mutant progenitors after 72 hr exposure to rapamycin (300×).
(D) Tuj1-IR neurons and GFAP-IR astrocytes derived from control and mutant progenitors after FBS addition (200×). pS6 immunoreactivity in differentiated lines (300×, 600×) is shown. Most cells in differentiated mutant cultures activate mTORC1, as shown by pS6 activation (magnification 300×).
(E) GalC-IR oligodendrocytes derived from control and mutant progenitors after FBS addition (200×).
(F) Increased frequency of apoptotic cells in FGF2-stimulated mutant Tuj1-IR progenitor cells, as detected by cleaved-caspase 3 (Casp3).
(G) Differentiating (3 days FGF2) RhebQ64L-transduced eNSCs gave rise to Tuj1-IR cells that were $pS6_{S235/6}$ and FLAG positive (inserts). Differentiated (5 days FBS) RhebQ64L-transduced eNSCs contained aberrant Tuj1-IR cells. Tuj1-IR cells showing a normal morphology in RhebQ64L-transduced cultures (white arrow) were FLAG negative, i.e., derived from untransduced cells. Only Tuj1/FLAG-IR cells were counted in mutant eNSCs.
(H) Increased differentiation of naive eNSCs exposed to LIF in the presence of FGF2 for 3 days.
Error bars, SEM. See also Table S2 and Figure S3.

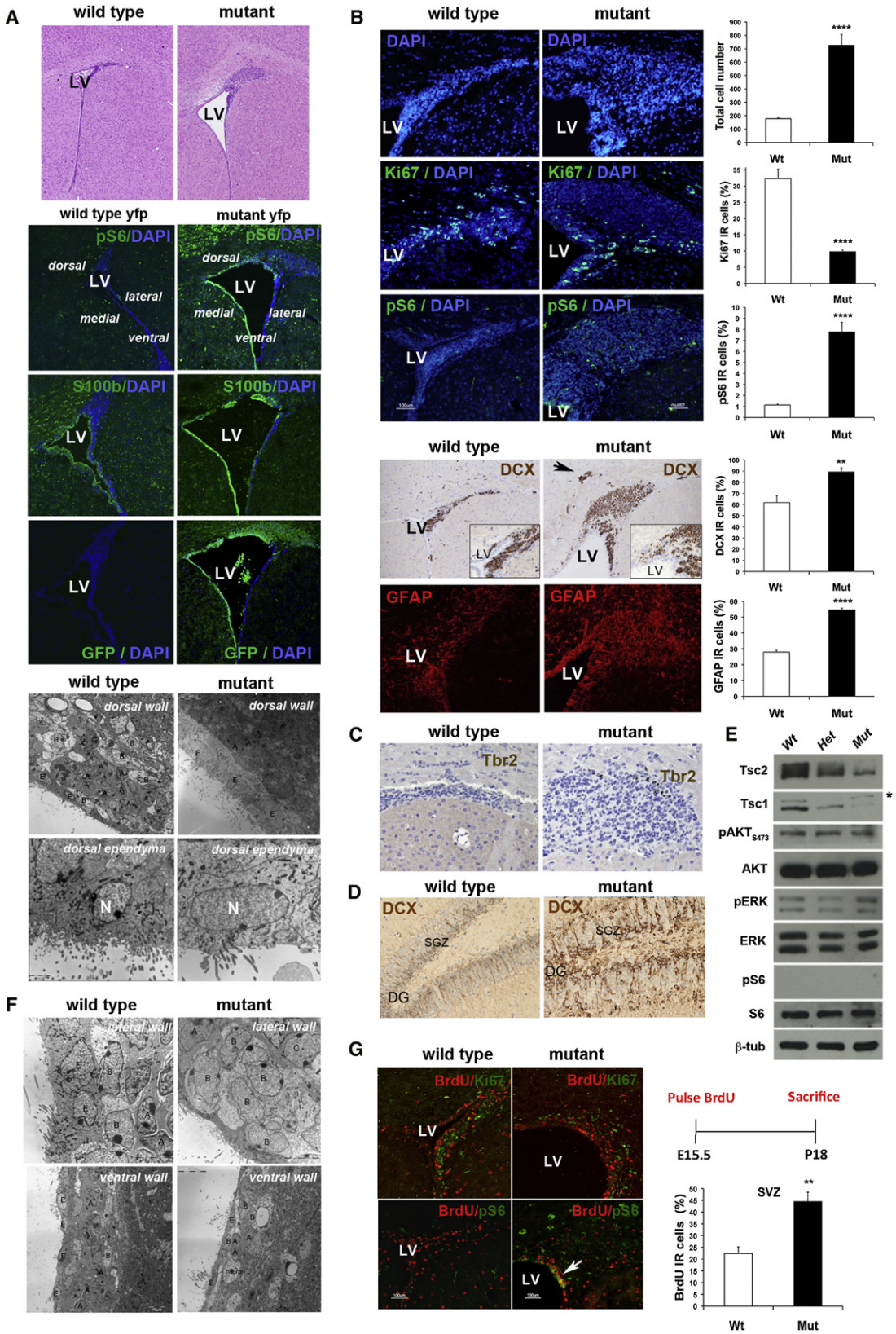
A
wild type
mutant
LV
wild type yfp
mutant yfp
pS6/DAPI
dorsal
lateral
medial
ventral
S100b/DAPI
GFP / DAPI
dorsal wall
dorsal ependyma
N
F
lateral wall
ventral wall
B
DAPI
Ki67 / DAPI
pS6 / DAPI
DCX
GFAP
Total cell number
Ki67 IR cells (%)
pS6 IR cells (%)
DCX IR cells (%)
GFAP IR cells (%)
Wt
Mut
C
Tbr2
D
SGZ
DG
E
Wt
Het
Mut
Tsc2
Tsc1
pAKT S473
AKT
pERK
ERK
pS6
S6
β-tub
G
BrdU/Ki67
BrdU/pS6
Pulse BrdU
Sacrifice
E15.5
P18
SVZ
BrdU IR cells (%)

many GFAP-IR cells (Figure 5B and Table S3). Ectopic Tbr2-IR cells were also retrieved at the peripheral-most edges (Figure 5C). Notably, DCX-IR progenitors were found at increased numbers and in ectopic locations also in the mutant SGZ of the DG (Figure 5D). Mutant SVZ showed significant reduction in both Tsc1 and Tsc2 proteins, with no activation in pS6 or difference in pERK or pAkt (Figure 5E).

Whereas accumulation of Type A neuroblasts could be detected dorsally, alterations in Type B SC distribution were observed along the entire wall of the SVZ (Figure 5F). Indeed, Type B and Type B1 cells, i.e., the subset contacting the ventricle with the primary cilium, were large, with many nuclear membrane fusions, and accumulated in the dorsal and lateral SVZ as cell clusters. Type C transit progenitors were not affected. Aberrant niche organization could be detected also in ventral regions, where SVZ was not observed. Given that progenitors in the dorsal SVZ should normally migrate from dorsolateral to ventral striatal SVZ (Kakita and Goldman, 1999), mTOR hyperactivation in early postnatal SVZ progenitors might have impaired their migration ventrally, eventually contributing to the development of the aberrant dorsal mass.

To assess whether altered proliferation of mutant embryonic SCs might be responsible for the aberrant expansion of postnatal SVZ progenitors, a "birth-dating" experiment was adapted to comply with the early lethality of mutant mice. BrdU was given at E15.5 and litters were sacrificed at P18. A 20% increase in the percentage of BrdU-retaining cells could be detected in P18 mutant dorsolateral SVZ, with some BrdU-retaining cells being also pS6 IR (n = 3) (Figure 5G).

A massive enlargement of the dorsal SVZ was observed protruding into the ventricle as early as at P0 all throughout P18 (Figure 6 and Table S3) and was GFP-positive, and thus Cre-recombined (Figure 6A). This ectopic cell mass invaded the prospective corpus callosum (CC) region, forcing amyelinic axons, which in controls clearly delimited the SVZ, to project far away from the ventricular surface (Figure 6B).

The frequency of Ki67 cells in mutant VZ/SVZ was higher at embryonic and early postnatal stages (E16.5 and P0) than late postnatally (P7 and P15), indicating a progressive decline in the proliferative ability of mutant SVZ progenitors (Figure 2D, Figure 5B, Figure 6C, and Table S3). To confirm these findings, mice were given pulses of BrdU every 12 hr from P5 to P7. P7 mutant SVZ contained a lower fraction of BrdU-IR cells than that of controls (33.9% ± 1.5% and 14.8% ± 1.2% in WT and mutant SVZ, respectively; $p < 0.01$), confirming reduced proliferation capacity of postnatal mutant SVZ progenitors, as in SENs. Also, pS6 remained consistently higher in mutants at P0, while decreasing at P7 and P15 (Figure 6D and Table S3).

Both hydrocephalus and abnormal expansion of dorsal SVZ were reverted in rapamycin-treated mutant mice, but did not reoccur upon rapamycin suspension, in spite of pS6 reactivation (Figure 6E). Interestingly, Gpnmb, previously found to be overexpressed in mutant eNSCs and human SEGAs (Figures 3O and 3P), was detected also in aberrant mutant SVZ expansion (Figure 6F), reinforcing the hypothesis that this region truly recapitulated human SEN. Remarkably, pSTAT3 activation was also observed in mutant cortex, SVZ, and hippocampus (Figure 6G).

To assess if postnatal mutant SVZ NSCs were also characterized by premature differentiation, we established NSC lines at P7 and P18. None of the mutant SVZ NSC lines showed Cre-mediated *Tsc1* loss, suggesting that Cre-recombined dorsal SVZ NSCs, characterized by low proliferation rate in vivo (Figure 5B and Figure 6C), were likely taken over in vitro by fast-proliferating NSCs from nonrecombined SVZ regions, which could not be excluded from the dissected tissue. To overcome this limitation, we enforced the expression of RhebQ64L in naive P15 SVZ NSCs (Figure S4), which, as E16.5 NSCs, displayed premature differentiation into neuronal and glial cells and impaired terminal neuronal maturation.

Loss of *Tsc1* Expression during Embryonic Development Led to Defects in Neuronal Migration along the Rostral Migratory Stream

The mutant rostral migratory stream (RMS) contained a high frequency of pS6-IR cells, few peripherally localized KI67-IR cells, and multiple layers of DCX-IR cells (Figure 7). Interestingly, remnants of the olfactory ventricle, which should have disappeared by P3, were still detected in the center of the mutant RMS. Uniciliated and multiciliated cells, located around the olfactory ventricle at P7 and P15, respectively, displayed features typical of immature radial glia cells, such as disorganized microtubules and abundant smooth ER. Nuclear distribution profiles at P15 indicated that mutant RMS cells dispersed throughout the parenchyma, while in controls, they were organized in compact clusters (Figure 7B). EM analysis showed that mutant RMS neuroblasts at P7 were very tightly associated and did not migrate properly, while at P15 they displayed few union complexes, thus migrating mostly as single cells or in small cell clusters.

In agreement with the impaired migration ability of mutant RMS neuroblasts, the anatomical targets of RMS migration,

Figure 5. Loss of *Tsc1* Expression during Embryonic Development Severely Impairs the Organization of the Postnatal SVZ Niche

(A) Enhanced dilatation of ventricles in mutant brains at P15 (H&E). Recombination of *Tsc1* allele in the dorsal and medial walls by GFP expression and pS6 in *Tsc1*$^{c/-}$/*Emx1-Cre*$^{+}$/*RosaR-YFP* mice is shown. S100β expression in control and mutant ventricles (100×, 200×) is also shown, as is EM of dorsal wall and dorsal ependyma. N, nucleus.

(B) DAPI counterstaining showing increased number of cells in dorsolateral corner of SVZ. SVZ proliferation (Ki67), mTORC1 activation (pS6), and Type A progenitor marker doublecortin (DCX) expression in the dorsal SVZ is shown. Arrow indicates a DCX-IR heterotopia. High frequency of GFAP-IR cells in mutant dorsal SVZ (100×, 200×) is evident.

(C) Tbr2-IR cells are retrieved at the edge of the massive expansion (200×).

(D) Increased numbers of DCX-IR neuronal progenitors in the mutant SGZ of the DG at P15 (magnification 200×). DG, dentate gyrus; SGZ, subgranular zone.

(E) mTOR activation analysis performed by western blot on P15 SVZ tissues (n = 3). (*), aspecific band for TSC1.

(F) Enlarged and immature Type B cells in the lateral and ventral wall of the mutant ventricle (by EM).

(G) BrdU-IR cell quantification in the dorsolateral SVZ at P18, after BrdU pulse at E15.5. BrdU/pS6-IR cells in the mutant SVZ are indicated by an arrow.

Error bars, SEM. See also Table S3 and Figure S4.

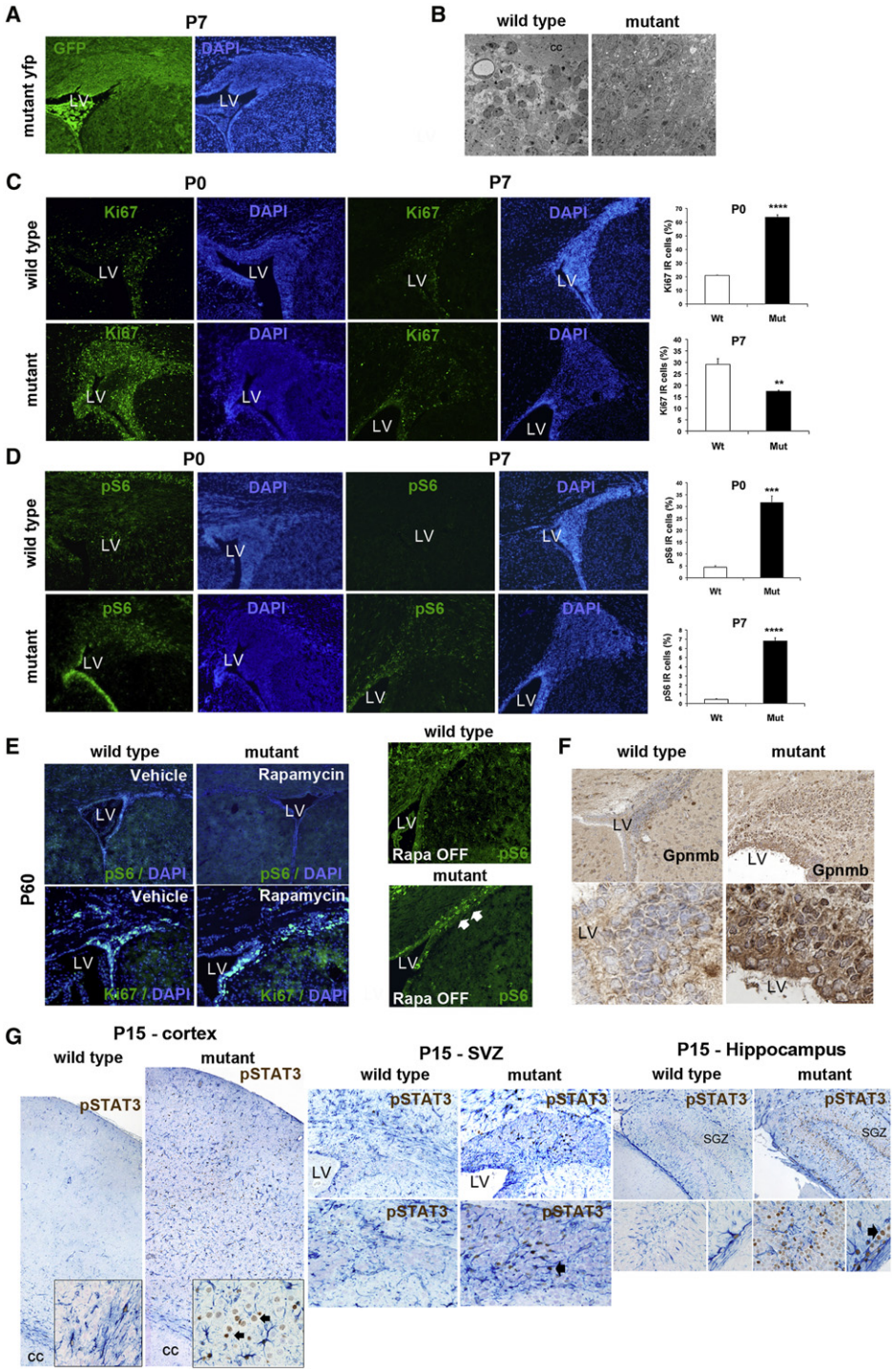

Figure 6. Late Postnatal Mutant SVZ Progenitors Were Endowed with Reduced Proliferation Ability

(A) Recombination of *Tsc1* allele by GFP staining in the mutant aberrant expansion at P7 (100×). LV, lateral ventricle.

(B) EM analysis of the tumor-like lesion in mutant SVZ at P7.

(C) Proliferation rate in the aberrant expansion by Ki67 staining at P0 and P7 (100×).

(D) Higher pS6 in mutant P0 and P7 SVZ (100×).

(E) Chronic rapamycin treatment reduced both hydrocephalus and dorsal SVZ mass (P60), which did not reoccur after rapamycin suspension, in spite of pS6 reactivation (Rapa OFF; pS6-IR cells, arrow).

(F) Gpnmb expression in the SVZ expansion of P15 mutant mice.

(G) pSTAT3 activation in P15 mutant cortex, SVZ, and hippocampus (arrow, pSTAT3-IR cells).

Error bars, SEM. See also Table S3.

i.e., the OBs, were highly affected in mutants (Figure 7C). As shown by H&E and by Tbr2 and calretinin staining, the mitral and the glomerular cell layers were disorganized, with the granule cell layer being highly expanded. In line with the above findings, treatment of mutant mice with rapamycin also reverted the RMS phenotype (Figure 7D).

Taken together, these results suggest that SVZ Type A *Tsc1*-deficient neuroblasts, which were produced in excess by Type B cells, did not mature properly and were not capable of sustaining proper chain migration (Figure 7E).

DISCUSSION

mTOR Activation in Embryonic Progenitors Deregulates Self-Renewal and Differentiation, Leading to Alterations in Embryonic and Postnatal NSC Compartments In Vivo

Maintenance of different somatic tissues is dependent on the presence of a resident SC pool with self-renewal potential that generates differentiating progeny. The balance between self-renewal and differentiation needs to be finely tuned to ensure proper tissue homeostasis. Accumulating evidence suggests that persistent mTORC1 activation in SC compartments leads to increased SC proliferation followed by SC exhaustion (Gan et al., 2008; Sun et al., 2010; Castilho et al., 2009). Accordingly, *Tsc1* deletion in *Emx1*-expressing neuroepithelial cells resulted in the transient expansion of both VZ and SVZ progenitors during mid-late cortical neurogenesis due to alterations in the symmetry of differentiative/neurogenic divisions. This cell amplification contributed to the expansion of most cortical layers and to megalencephaly, and was followed by a progressively reduced mitotic activity of NSCs postnatally. Of note, the functional terminal maturation of the excessively generated mutant neuronal cells was defective, as indicated by the presence of aberrant SMI311-IR neurons, by downregulation of markers of mature neurons, and by development of seizures. At the same time, the deregulated proliferation of embryonic VZ/SVZ NSC compartment was responsible for the deranged homeostasis of the postnatal SVZ niche, which resulted in the formation of ectopic periventricular masses, mostly composed of neuroblasts. Again, correct maturation and specialization of postnatal RMS neuroblasts was negatively affected by *Tsc1* loss, because the OBs were severely reduced in size and highly disorganized.

Notably, the developmental defects observed in our mutant mice were different from those described in most mouse models of TSC. Only recently, *Tsc2* loss in radial glial cells at E13.5 by *hGFAP-Cre* recombination resulted in the generation of a mouse model that more closely mimicked TSC-associated alterations (Way et al., 2009). Whereas this study reported that the increase in cortical thickness arose postnatally, we detected it at E16.5, in line with the embryonic origin of cortical alterations in TSC patients (Holmes and Stafstrom, 2007). The difference in timing and onset of alterations in cortical thickness implies the involvement of different neural cell lineages: during embryogenesis, hyperactivation of mTOR increased the generation of cells belonging to the neuronal lineage, whereas persistent activation of the pathway postnatally contributed to cortical remodeling, likely by promoting an increase in reactive astrocytes.

Likewise, whereas reduced expression of the postmitotic neuronal marker Tbr1 in layer VI cells in P15 mutants was explained by Way et al. (2009) as the result of lower numbers of neurons generated during embryogenesis, we demonstrated that this was due to defects in terminal neuronal maturation.

Remarkably, while taking into account that the in vitro milieu does not fully reproduce the variety of signals retrieved in vivo, some in vivo features of $Tsc1^{c/c}$/*Emx1-Cre*$^{+}$ mice, such as the progressively reduced NSC proliferation, their premature neuronal differentiation, and impaired maturation, were also observed in E16.5 mutant eNSCs when expanded ex vivo as neurospheres.

mTORC1 Activation Controls Self-Renewal and Neuronal Differentiation in eNSCs In Vitro by Modulating Akt and STAT3 Pathways

Our in vitro observations are in partial agreement with findings in *Tsc2* null neuroepithelial progenitors (NEPs) at E10.5 (Onda et al., 2002). In fact, ectopic expression of GFAP and increased cell size were detected also in NEPs. However, while enhanced proliferation was observed in *Tsc2* mutant NEPs, *Tsc1* mutant eNSCs undergo a dramatic reduction in self-renewal ability, likely due to the attenuation of the PI3K-Akt pathway, which was not reported in E10.5 NEPs. Indeed, reduced Akt phosphorylation in mutant eNSCs was mainly due to the activation of a regulatory mTORC1-dependent negative feedback loop, which was relieved by short rapamycin treatment. Accordingly, we did not find evidence of mTORC2 involvement.

Increasing Akt phosphorylation, by enforced Akt-1 expression, ROS stimulation, *Nf1* production, or *Pten* deletion (Sinor and Lillien, 2004; Le Belle et al., 2011; Dasgupta and Gutmann, 2005; Gregorian et al., 2009), results in enhanced NSC proliferation and self-renewal, although this effect might be cell and stage specific (Bonaguidi et al., 2011). Correspondingly, reduced Akt activity by mTORC1-dependent regulatory feedback in mutant NSCs negatively controls their self-renewal ability in vivo and in vitro. Interestingly, Akt hypophosphorylation might counteract the activation of proproliferative mediators, such as *c-myc* (Gregory et al., 2003), which we showed to be hyperfunctional upon *Tsc1* haploinsufficiency in vitro. As opposed to neurofibromatosis (NF), in which haploinsufficiency induces phenotypic abnormalities in patients and animal models (Dasgupta and Gutmann, 2005), the eNSC *Tsc1* haploinsufficient phenotype in vitro doesn't have an in vivo correlate. This is in agreement with the requirement for somatic second hit *TSC1* or *TSC2* mutations for tuber formation in TSC patients (Crino et al., 2010).

We identified the transcription factor STAT3 as a central player in inducing premature neuronal and astroglial differentiation in *Tsc1* mutant eNSCs. STAT3 phosphorylation on Ser727, which allows transcriptional activation, is directly regulated by mTOR (Yokogami et al., 2000). Accordingly, $pSTAT3_{Ser727}$ is activated in about 50% of mutant eNSCs under proliferative conditions, and STAT3 activation by ligand stimulation results in the same precocious generation of differentiated progeny. Overall, STAT3 activation might be the link between mTOR hyperactivation and premature eNSC differentiation. Indeed, STAT3 is also highly phosphorylated in the cortex, the SVZ, and the hippocampus of our mutant mice in vivo, as well as in patients' CTs and SEGAs (Baybis et al., 2004; Chan et al., 2004). Accordingly, STAT3 transcriptional target genes, such as *GFAP* and *SerpinA3*, are found

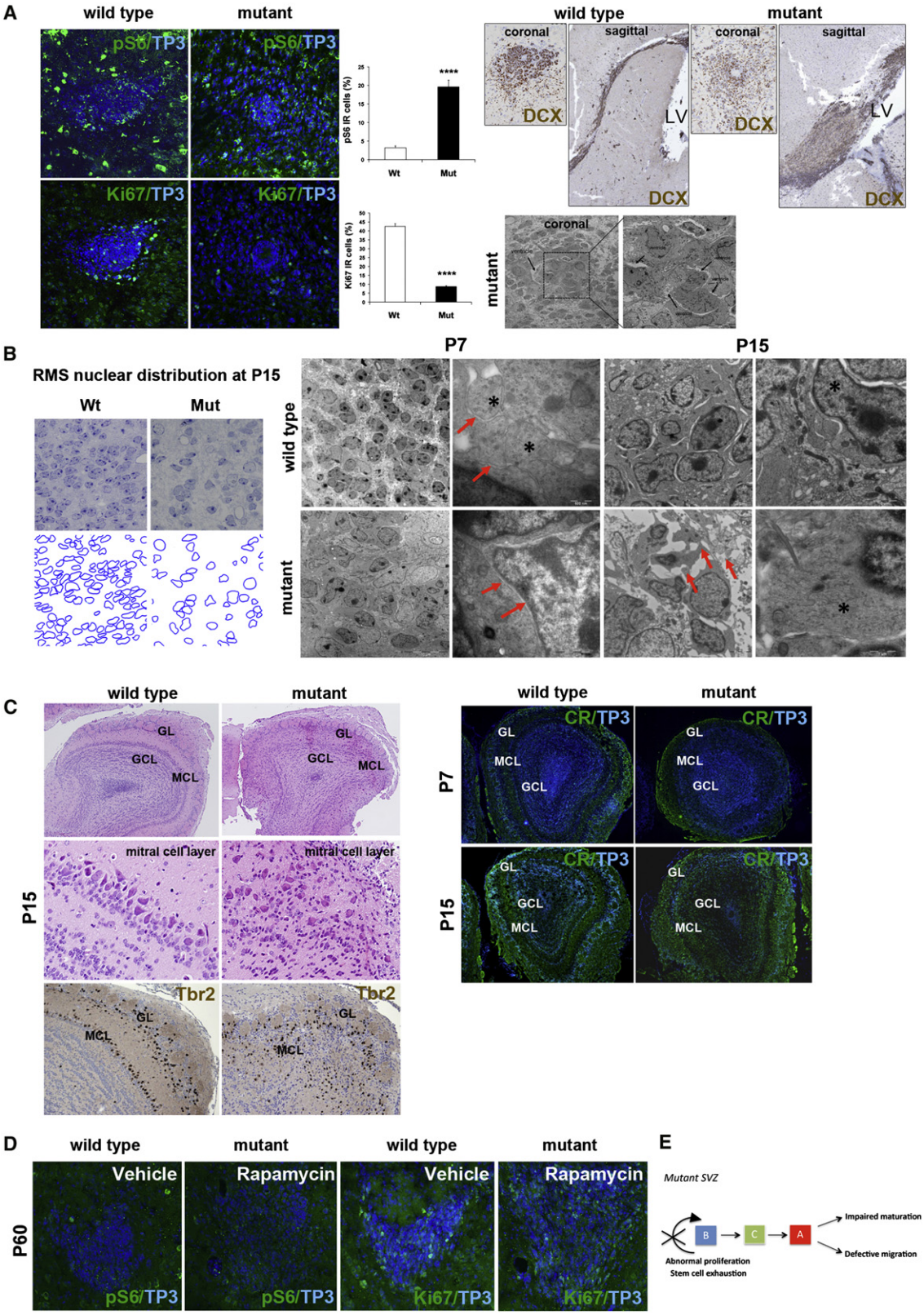

Figure 7. Loss of *Tsc1* Expression during Embryonic Development Led to Defects in Neuronal Migration along the RMS

(A) DAPI staining and pS6 in control and mutant rostral migratory stream (RMS) at P15. Ki67 proliferating cells can be seen at the borders of the mutant RMS. DCX staining in RMS (coronal and sagittal sections, 100× and 40×, respectively) is shown, as is mutant RMS containing remnants of the ventricle at P15 (by EM).

to be significantly overexpressed in mutant eNSCs and TSC lesions (Ess et al., 2004).

In the end, self-renewal, proliferation, and differentiation of NSCs are finely orchestrated by different intracellular pathways (i.e. PI3K/Akt and STAT3), which depend directly on mTOR, confirming its pivotal role in controlling NSC biology.

EXPERIMENTAL PROCEDURES

Generation of *Tsc1* Floxed/*Emx1-Cre* Mice

To generate $Tsc1^{c/-}$*Emx1-Cre* and $Tsc1^{c/c}$*Emx1-Cre* animals, mixed background (129S4/SvJae, C57BL/6) $Tsc1^{c/-}$ mice or $Tsc1^{c/c}$ mice (Jackson) were intercrossed with *Emx1-Cre* heterozygous mice. We used (c), (WT), and (−) to denote the conditional (floxed), WT, and null alleles of *Tsc1*, respectively; the formal name of the c allele is *Tsc1tm1Djk*. *Tsc1* mutants were genotyped by tail-derived gDNA PCR by using primers described previously (Uhlmann et al., 2002b). All animal experiments were approved by and performed in accordance with the guidelines of the International Animal Care and Use Committee.

Immunostaining on Paraffin-Embedded and Frozen Sections

Brains from embryos or from intracardially perfused postnatal mice were fixed for 24 hr in 4% PFA. Sixteen-micron frozen sections were directly incubated with primary Abs. From paraffin-embedded brains, 5 μm paraffin sections were obtained, deparaffinized, rehydrated, treated for antigen retrieval, and incubated in 10% serum blocking solution prior to incubation with primary antibodies. See Supplemental Experimental Procedures for the list of primary antibodies.

Cell Cycle Exit and BrdU Birth-Dating Experiments

For cell cycle exit, timed, pregnant mice were injected with BrdU (Sigma) intraperitoneally at 40 mg/g body weight at E15.5 and sacrificed at E16.5. For BrdU birth-dating, timed, pregnant mice were injected with BrdU at E15.5 and sacrificed at P18. For BrdU staining, sections were treated with 2N HCl for 20 min at RT followed by two washes with 0.1 M boric acid (pH 8.5) for 10 min at RT prior to blocking. The primary antibody used was rat anti-BrdU (Serotec).

Immunoblotting

Cortical tissues from embryos and cortical/SVZ tissues from postnatal mice were dissected out and directly stored at −80°C. Each frozen tissue was homogenized in 10× volume of RIPA lysis buffer (10 mM Tris-Cl [pH 7.2], 150 mM NaCl, 1 mM EDTA [pH 8]) with 1% Triton X-100, 1% deoxycholate, 0.1% SDS, and protease and phosphatase inhibitor mixture (Roche). Samples were prepared according to standard western blotting protocol. See Supplemental Experimental Procedures for details.

Isolation and Characterization of NSCs from WT and Mutant Mice

NSC cultures were established under mild hypoxic (5% O_2) culture conditions from the E16.5 cortex of WT and mutant mice. For population analysis, cells were plated at 8×10^3 cells/cm^2, and the formed spheres were collected every 3–5 days. For clonogenic assays, cells derived from the dissociation of clonal single neurospheres were seeded in 96-well plates, and the number of secondary spheres generated was assessed after 8–10 days.

Differentiation of NSC Cultures

To evaluate multipotency, NSCs were treated as in Parras et al. (2004). For the experiment with LIF (Peprotech), naive eNSCs were plated in standard media with or without 10 ng/ml LIF.

Lentiviral Vector Generation and Cell Infection

RhebQ64L construct (kindly provided by Drs. Jiang and Vogt; The Scripps Research Institute, La Jolla, CA, USA) was cloned into a monocistronic transfer lentiviral vector pCCL.sin.cPPT.PGK.GFP.WPRE11, after removal of the GFP cassette. eNSCs were transduced with 1×10^7 TU/ml of lentiviral vectors for 16 hr. Infection efficiency was assessed by counting the frequency of FLAG-IR cells and by western blotting for FLAG.

Treatment with Rapamycin

For in vivo administration, rapamycin (LC-Labs, USA) was dissolved in 100% ethanol, stored at −20°C, and diluted in a vehicle solution containing 5% Tween 80 and 5% PEG 400 (Sigma, St. Louis, MO) immediately before injection. Mice were intraperitoneally injected with 6 mg/kg of drug or vehicle every 2 days. For in vitro treatment, rapamycin was dissolved in DMSO and used at a final concentration of 100 nM in medium.

Molecular Analysis

Total RNA from eNSCs lines was extracted using the RNeasy Mini Kits (QIAGEN). cDNA was obtained by using Omniscript RT Kit (QIAGEN). All cDNAs were normalized to the β-actin RT-PCR product. For microarray analysis, refer to Supplemental Experimental Procedures.

Statistical Analysis

Results for continuous variables were expressed as mean ± standard error of the mean (SEM). Two-group comparisons were performed with the independent samples' Student t test. $p < 0.05$ was considered statistically significant. *$p < 0.05$; **$p < 0.01$; ***$p < 0.005$; ****$p < 0.001$.

SUPPLEMENTAL INFORMATION

Supplemental Information for this article includes four figures, three tables, two lists, and Supplemental Experimental Procedures and can be found with this article online at doi:10.1016/j.stem.2011.09.008.

ACKNOWLEDGMENTS

This work was supported by Associazione Sclerosi Tuberosa (AST) to R.G. We thank Paolo Caferra for help and assistance with molecular analysis and Luca Muzio for critical reading of the manuscript.

Received: January 16, 2011
Revised: June 20, 2011
Accepted: September 15, 2011
Published: November 3, 2011

REFERENCES

Baybis, M., Yu, J., Lee, A., Golden, J.A., Weiner, H., McKhann, G., 2nd, Aronica, E., and Crino, P.B. (2004). mTOR cascade activation distinguishes tubers from focal cortical dysplasia. Ann. Neurol. *56*, 478–487.

Bonaguidi, M.A., Wheeler, M.A., Shapiro, J.S., Stadel, R.P., Sun, G.J., Ming, G.L., and Song, H. (2011). In vivo clonal analysis reveals self-renewing and multipotent adult neural stem cell characteristics. Cell *145*, 1142–1155.

Castilho, R.M., Squarize, C.H., Chodosh, L.A., Williams, B.O., and Gutkind, J.S. (2009). mTOR mediates Wnt-induced epidermal stem cell exhaustion and aging. Cell Stem Cell *5*, 279–289.

Chan, J.A., Zhang, H., Roberts, P.S., Jozwiak, S., Wieslawa, G., Lewin-Kowalik, J., Kotulska, K., and Kwiatkowski, D.J. (2004). Pathogenesis of

(B) Diagrams showing the RMS cellular organization by toluidine-blue-stained semithin sections at P15. EM analysis of control and mutant RMS at P7 and P15 (red arrow, intercellular spaces; [*]: migrating neuroblasts) is shown.
(C) H&E, Tbr2, and calretinin staining of OBs showing disorganization of mitral and glomerular layers (40×, 100×, 600×). MCL, mitral cell layer; GL, glomerular layer; GCL, granule cell layer.
(D) pS6 and Ki67 staining after chronic rapamycin treatment (40×).
(E) Model summarizing cell lineage defects in the mutant SVZ.
Error bars, SEM.

tuberous sclerosis subependymal giant cell astrocytomas: biallelic inactivation of TSC1 or TSC2 leads to mTOR activation. J. Neuropathol. Exp. Neurol. *63*, 1236–1242.

Crino, P.B., Nathanson, K.L., and Henske, E.P. (2006). The tuberous sclerosis complex. N. Engl. J. Med. *355*, 1345–1356.

Crino, P.B., Aronica, E., Baltuch, G., and Nathanson, K.L. (2010). Biallelic TSC gene inactivation in tuberous sclerosis complex. Neurology *74*, 1716–1723.

Dasgupta, B., and Gutmann, D.H. (2005). Neurofibromin regulates neural stem cell proliferation, survival, and astroglial differentiation in vitro and in vivo. J. Neurosci. *25*, 5584–5594.

Ehninger, D., Han, S., Shilyansky, C., Zhou, Y., Li, W., Kwiatkowski, D.J., Ramesh, V., and Silva, A.J. (2008). Reversal of learning deficits in a Tsc2+/- mouse model of tuberous sclerosis. Nat. Med. *14*, 843–848.

Ess, K.C., Uhlmann, E.J., Li, W., Li, H., Declue, J.E., Crino, P.B., and Gutmann, D.H. (2004). Expression profiling in tuberous sclerosis complex (TSC) knockout mouse astrocytes to characterize human TSC brain pathology. Glia *46*, 28–40.

Gan, B., Sahin, E., Jiang, S., Sanchez-Aguilera, A., Scott, K.L., Chin, L., Williams, D.A., Kwiatkowski, D.J., and DePinho, R.A. (2008). mTORC1-dependent and -independent regulation of stem cell renewal, differentiation, and mobilization. Proc. Natl. Acad. Sci. USA *105*, 19384–19389.

Gorski, J.A., Talley, T., Qiu, M., Puelles, L., Rubenstein, J.L., and Jones, K.R. (2002). Cortical excitatory neurons and glia, but not GABAergic neurons, are produced in the Emx1-expressing lineage. J. Neurosci. *22*, 6309–6314.

Gregorian, C., Nakashima, J., Le Belle, J., Ohab, J., Kim, R., Liu, A., Smith, K.B., Groszer, M., Garcia, A.D., Sofroniew, M.V., et al. (2009). Pten deletion in adult neural stem/progenitor cells enhances constitutive neurogenesis. J. Neurosci. *29*, 1874–1886.

Gregory, M.A., Qi, Y., and Hann, S.R. (2003). Phosphorylation by glycogen synthase kinase-3 controls c-myc proteolysis and subnuclear localization. J. Biol. Chem. *278*, 51606–51612.

Hobbs, R.M., Seandel, M., Falciatori, I., Rafii, S., and Pandolfi, P.P. (2010). Plzf regulates germline progenitor self-renewal by opposing mTORC1. Cell *142*, 468–479.

Holmes, G.L., and Stafstrom, C.E.; Tuberous Sclerosis Study Group. (2007). Tuberous sclerosis complex and epilepsy: recent developments and future challenges. Epilepsia *48*, 617–630.

Jozwiak, J., Jozwiak, S., and Wlodarski, P. (2008). Possible mechanisms of disease development in tuberous sclerosis. Lancet Oncol. *9*, 73–79.

Kakita, A., and Goldman, J.E. (1999). Patterns and dynamics of SVZ cell migration in the postnatal forebrain: monitoring living progenitors in slice preparations. Neuron *23*, 461–472.

Le Belle, J.E., Orozco, N.M., Paucar, A.A., Saxe, J.P., Mottahedeh, J., Pyle, A.D., Wu, H., and Kornblum, H.I. (2011). Proliferative neural stem cells have high endogenous ROS levels that regulate self-renewal and neurogenesis in a PI3K/Akt-dependant manner. Cell Stem Cell *8*, 59–71.

Meikle, L., Talos, D.M., Onda, H., Pollizzi, K., Rotenberg, A., Sahin, M., Jensen, F.E., and Kwiatkowski, D.J. (2007). A mouse model of tuberous sclerosis: neuronal loss of Tsc1 causes dysplastic and ectopic neurons, reduced myelination, seizure activity, and limited survival. J. Neurosci. *27*, 5546–5558.

Onda, H., Crino, P.B., Zhang, H., Murphey, R.D., Rastelli, L., Gould Rothberg, B.E., and Kwiatkowski, D.J. (2002). Tsc2 null murine neuroepithelial cells are a model for human tuber giant cells, and show activation of an mTOR pathway. Mol. Cell. Neurosci. *21*, 561–574.

Orlova, K.A., Tsai, V., Baybis, M., Heuer, G.G., Sisodiya, S., Thom, M., Strauss, K., Aronica, E., Storm, P.B., and Crino, P.B. (2010). Early progenitor cell marker expression distinguishes type II from type I focal cortical dysplasias. J. Neuropathol. Exp. Neurol. *69*, 850–863.

Parras, C.M., Galli, R., Britz, O., Soares, S., Galichet, C., Battiste, J., Johnson, J.E., Nakafuku, M., Vescovi, A., and Guillemot, F. (2004). Mash1 specifies neurons and oligodendrocytes in the postnatal brain. EMBO J. *23*, 4495–4505.

Ridler, K., Suckling, J., Higgins, N., Bolton, P., and Bullmore, E. (2004). Standardized whole brain mapping of tubers and subependymal nodules in tuberous sclerosis complex. J. Child Neurol. *19*, 658–665.

Schmidt, E.V., Ravitz, M.J., Chen, L., and Lynch, M. (2009). Growth controls connect: interactions between c-myc and the tuberous sclerosis complex-mTOR pathway. Cell Cycle *8*, 1344–1351.

Sinor, A.D., and Lillien, L. (2004). Akt-1 expression level regulates CNS precursors. J. Neurosci. *24*, 8531–8541.

Sun, P., Quan, Z., Zhang, B., Wu, T., and Xi, R. (2010). TSC1/2 tumour suppressor complex maintains Drosophila germline stem cells by preventing differentiation. Development *137*, 2461–2469.

Uhlmann, E.J., Apicelli, A.J., Baldwin, R.L., Burke, S.P., Bajenaru, M.L., Onda, H., Kwiatkowski, D., and Gutmann, D.H. (2002a). Heterozygosity for the tuberous sclerosis complex (TSC) gene products results in increased astrocyte numbers and decreased p27-Kip1 expression in TSC2+/- cells. Oncogene *21*, 4050–4059.

Uhlmann, E.J., Wong, M., Baldwin, R.L., Bajenaru, M.L., Onda, H., Kwiatkowski, D.J., Yamada, K., and Gutmann, D.H. (2002b). Astrocyte-specific TSC1 conditional knockout mice exhibit abnormal neuronal organization and seizures. Ann. Neurol. *52*, 285–296.

Way, S.W., McKenna, J., 3rd, Mietzsch, U., Reith, R.M., Wu, H.C., and Gambello, M.J. (2009). Loss of Tsc2 in radial glia models the brain pathology of tuberous sclerosis complex in the mouse. Hum. Mol. Genet. *18*, 1252–1265.

Yokogami, K., Wakisaka, S., Avruch, J., and Reeves, S.A. (2000). Serine phosphorylation and maximal activation of STAT3 during CNTF signaling is mediated by the rapamycin target mTOR. Curr. Biol. *10*, 47–50.

Young, K.M., Fogarty, M., Kessaris, N., and Richardson, W.D. (2007). Subventricular zone stem cells are heterogeneous with respect to their embryonic origins and neurogenic fates in the adult olfactory bulb. J. Neurosci. *27*, 8286–8296.